Journal of Materials Chemistry A

Accepted Manuscript

ROYAL SOCIETY OF CHEMISTRY

www.rsc.org/materialsA

Journal Name

ARTICLE

Two-dimensional net-like SnO_2/ZnO heteronanostructures for high-performance H_2S gas sensor †

Received 00th January 20xx,
Accepted 00th January 20xx

DOI: 10.1039/x0xx00000x

www.rsc.org/

Diyu Fu,[a,c] Chunling Zhu,*[b] Xitian Zhang, [c] Chunyan Li [a] and Yujin Chen*[a]

H_2S gas even with a low concentration (20 ppb) in the environment is very harmful to the health of human beings. Therefore, the design and fabrication of gas sensors for detecting trace H_2S gas in the environment are highly desirable. However, it remains a challenge to develop gas sensors that can detect H_2S with a concentration at ppb level at a relatively low temperature. Herein we developed a facile method to fabricate two-dimensional net-like SnO_2/ZnO heteronanostructures with a porous feature. Compared to net-like SnO_2 and ZnO homonanostructures, the sizes of both SnO_2 and ZnO in the net-like heteronanostruces were decreased significantly. Specially, heterojunctions formed at the interfaces between SnO_2 and ZnO. As a result, the net-like SnO_2/ZnO heteronanostructures exhibited superior H_2S sensing properties including higher sensor response, and better selectivity and long-term stability to net-like SnO_2 and ZnO homonanostructures, and other types of metal oxide-based nanocomposites. Importantly, the SnO_2/ZnO heteronanostructures could detect 10 ppb H_2S even at a working temperature of 100°C. Therefore, the net-like SnO_2/ZnO heteronanostructures have very promising applications in high-performance H_2S sensors. In addition, the fabrication method presented here is facile, repeatable and operable, and thus it may be extended to synthesize other-type metal oxides-based heteronanostructures for applications in various fields.

1 Introduction

Gas sensors based on metal oxide semiconductors (MOSs), such as SnO_2, CuO, WO_3 and ZnO, etc., have attracted much attention due to their high sensitivity, low cost, and simplicity in fabricating sensors.[1-4] Among them, n-type semiconductors have been studied extensively due to their faster surface reaction kinetics. In general, the sensing mechanism of individual n-type MOS is based on the change of the width of the electron depleted layer at different gas atmospheres.[5] As n-type MOS is exposed to air, oxygen molecules will adsorb on the MOS surface, and then extract electrons from the conductance band to form negative oxygen ion, leading to the formation of the electron depleted layer at the surface. When n-type MOS is exposed to reducing gases, the trapped electrons will be released to the conductance band owing to the reactions between reducing gases and adsorbed oxygen species, and then decrease the width of electron depleted layer. When the width of electron depleted layer for a given n-type MOS in air is closed to its Debye length, the n-type MOS would exhibit excellent sensing properties.[5-8] Thus, n-type MOS with a small size is highly desirable to improve its sensitivity to reducing gases. However, in terms of the sensing mechanism n-type MOS usually shows a comparable response to various kinds of reducing gases, especially to those with similar surface chemophysical properties. Therefore, the selectivity of individual n-type MOS is still unsatisfactory and limits its practical application in high-performance gas sensors.

Recently, heteronanostructures based on MOSs have been developed to fabricate high-performance gas sensors. Besides the synergistic effect (different MOSs have different response to target gases), heterojuction barrier formed at the interface plays an important role in the sensing property, and thus both sensitivity and selectivity of the sensors based MOS heteronanostructures were improved greatly.[9-29] To date, various types of heteronanostructrues based on MOSs including n/n [9-24] and n/p interfaces [25-29] have been fabricated through various methods. However, these studies are mainly focused on zero (0D) and one dimensional (1D) nanostructures, and two dimensional (2D) heteronanostructures have been reported scarcely. Compared to 0D and 1D heteronanostructures, more tightly contacted interfaces can be built up in the plane of 2D heteronanostrures by a rational structure designation, which facilitates the improvement of the sensing properties. In addition, porous or hollow MOS nanostructures have also very promising

[a] Key Laboratory of In-Fiber Integrated Optics, Ministry of Education and College of Science, Harbin Engineering University, Harbin 150001, China. E-mail: chenyujin@ hrbeu.edu.cn; Fax: +86-451-82519754; Tel: +86-451-82519754.
[b] College of Materials Science and Chemical Engineering, Harbin Engineering University, Harbin 150001, China. E-mail:zhuchunling@hrbeu.edu.cn
[c] Key Laboratory for Photonic and Electronic Bandgap Materials, Ministry of Education, and School of Physics and Electronic Engineering, Harbin Normal University, Harbin 150025, China.

†Electronic Supplementary Information (ESI) available: [EDX pattern of the heteronanostructures, nitrogen adsorption–desorption isotherms and the pore size distributions of the heteronanostructures and homonanostructures, stability of the heteronanostructures as H_2S sensors, comparison of sensing performance of the net-like heteronanostructures with other materials, and structural characterizations of SZ-2 and SZ-3 and the heteronanostructures before and after H_2S sensing test]. See DOI: 10.1039/x0xx00000x

applications in gas sensors because such structures allow more target gas molecules to diffusion in or out the sensing films, which boost the sensitivity and shorten response and recovery times of the sensors.[10-14, 28, 30] However, to our best knowledge, such 2D porous heteronanostructures have not been synthesized for high-performance gas sensors.

H_2S is one kind of the colorless and very poisonous gas that often produces in the sewage plants, coal mines and natural gas industries, and other industrially important hydrocarbon feedstock. The sensors that can detect the concentration of H_2S down to ppb level are highly desirable because the acceptable limit of H_2S for human beings is in the range of 20–100 ppb.[31] Recently, ZnO, SnO_2 and/or their composites have been used as sensing materials for H_2S sensors. Cao et al. reported that ZnO nanorods could detect 100 ppm H_2S with a response value of about 34.8 at 190°C.[32] Kim et al. have synthesized Pd-doped SnO_2-core/ZnO-shell nanorods and found that the sensors based on the nanorods could detect 20 ppm H_2S gas with the response value of 1.5 at room temperature.[33] Shewale et al. fabricated Sn doped ZnO films and observed that the sensor response of the thin films is about 1.4 to 30 ppm H_2S at 200 °C.[34] However, it remains a challenge to develop gas sensors that can detect H_2S with a concentration at ppb level at a relatively low temperature.

Herein we develop a facile strategy to fabricate 2D porous SnO_2/ZnO heteronanostructures using graphene sheets as hard templates by a facile method. The heteronanostructures show a net-like morphology with a high surface area. Furthermore, heterojunctions formed at the interfaces between SnO_2 and ZnO. As a result, compared to the SnO_2 and ZnO homonanostructures, the heteronanostructures exhibited significantly enhanced H_2S sensing properties including higher response and lower detection limit. Moreover, the SnO_2/ZnO heteronanostructures can detect 10 ppb H_2S even at a working temperature of 100°C. Thus, the SnO_2/ZnO heteronanostructures are good candidates for high-performance H_2S sensors. In addition, the simple fabrication method presented here may be extended to synthesize other-type MOS-based heteronanostructures for applications in various fields.

2 Experimental section

2.1 Synthesis of samples

2.1.1 Synthesis of net-like SnO_2 homonanostructures

Graphene/SnO_2 (G/SnO_2) composite was first synthesized by a wet-chemical method.[35] Typically, 10 mg of graphene was dispersed in 80 mL of deionized water by ultrasonic treatment for 30 min. Then 1.6 g of $SnCl_2{\cdot}2H_2O$ and 1.4 ml of HCl (37%) was dissolved in the as-obtained G suspension. The mixture above was kept at room temperature for 24 h under stirring. The precipitates were washed several times with distilled water and dried through a freeze-drying process. After heating G/SnO_2 composite at 500 °C for 2 h under ambient atmosphere, net-like SnO_2 homonanostructures were then obtained.

2.1.2 Synthesis of net-like ZnO homonanostructures

G/ZnO composite was first prepared by a wet-chemical method.[36,37] 1.4 g of zinc acetate ($Zn(CH_3COO)_2{\cdot}2H_2O$) was dispersed into 250 mL ethanol. After stirring for 15 min at 80°C, 0.4 g Lithium hydroxide (LiOH) were then added and dispersed by ultrasonic treatment for 10 min. 10 mg of graphene was added to the mixture above and then stirred at room temperature for 10 h. The precipitates were washed with distilled water, and dried through a freeze-drying process. After then treated at 500 °C for 2 h under ambient atmosphere, net-like ZnO homonanostructures were then obtained.

2.1.3 Synthesis of net-like SnO_2/ZnO heteronanostructures

0.7 g of $Zn(CH_3COO)_2{\cdot}2H_2O$ was dispersed into 125 mL ethanol. After stirring at 80°C for 15 min, 0.2 g LiOH were then added and dispersed by ultrasonic treatment for 10 min. 50 mg of G/SnO_2 composite was added to the mixture above and then stirred at room temperature for 10 h. The precipitates (G/SnO_2/ZnO) were washed with distilled water, and dried through a freeze-drying process. After heating the sample at 500 °C for 2 h, under the ambient atmosphere. After cooling to room temperature, net-like SnO_2/ZnO heteronanostructures were then synthesized.

2.2 Structure characterization

The morphology and size of samples were characterized by scanning electron microscope (HSD/SU70) and an FEI Tecnai-F20 transmission electron microscope equipped with a Gatan imaging filter (GIF). The crystal structure of the sample was determined by X-ray diffraction (D/max 2550 V, Cu Ka radiation). The pore diameter distribution and surface area were tested by nitrogen adsorption/desorption analysis (TRISTAR II3020). ICP mass spectrometry was measured by Thermo iCAP 6000 ICP-MS. X-ray photoelectron spectroscopy (XPS) were carried out by using a spectrometer with Mg Kα radiation (PHI 5700 ESCA System). The binding energy was calibrated with the C 1s position of contaminant carbon in the vacuum chamber of the XPS instrument (284.6 eV).

2.3 Sensor fabrication and the sensing measurements

The fabrication and testing principle of the gas sensor are similar to those described in our previous reports.[38] Simply, the sensing sample was dissolved in absolute ethanol, and a drop was spun on a ceramic tube between metal electrodes to form a thin film with a thickness of about 0.1 mm. A metal alloy coil through the ceramic tube was used to control the working temperature of the gas sensor. The gas sensing properties were tested by ZWS1-WS-30A system (Zhongxi yuanda Science and Technology Co., Ltd., China) with a test chamber of 18 L, a gas-intake window, 30 testing channels, and temperature controlled system. The standard tested gases were purchased from Beijing Kshergas Co., Ltd., China. A stationary state gas distribution method was used for testing the gas sensing properties. The sensor was placed in a test chamber full of fresh air at the beginning, and then a given amount of test gas was injected into the chamber by an injector. After the response reaching a steady value, the

sensor was exposed to ambient environment by opening the chamber. The sensor response (S) is denotened as S ($S = R_a/R_g$), where R_a is the sensor resistance in air and R_g is the resistance in target-air mixed gas, respectively. The response and recovery times were defined as the time needed for 90 and 80% of total resistance change after the sensor was exposed to the tested gas and air, respectively.

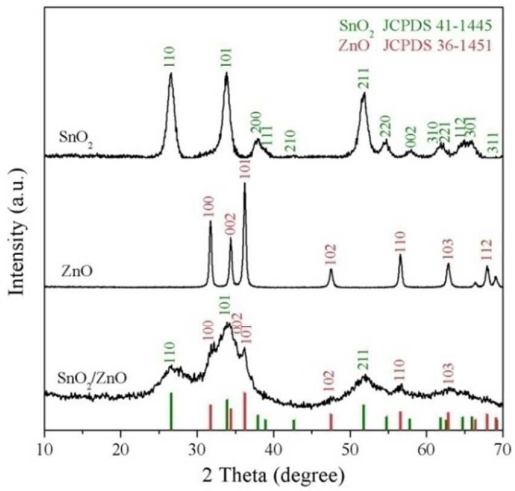

Figure 1 XRD patterns of net-like SnO_2 and ZnO homonanostructures and SnO_2/ZnO heteronanostructures.

3 Results and discussion

Figure 1 shows XRD patterns of the as-synthesized samples. The diffraction peaks labeled by Miller indices in the patterns of the net-like SnO_2 and ZnO homonanostructures can be indexed to tetragonal SnO_2 and hexagonal ZnO, respectively. No diffraction peaks from impurities are observed, suggesting high phase purities of SnO_2 and ZnO in the net-like homonanostructures, respectively. By careful analysis of the peaks in the XRD pattern of the net-like SnO_2/ZnO heteronanostructures, it can be found that both tetragonal SnO_2 and hexagonal ZnO are presented in the heteronanostructures. However, the diffraction peaks in the SnO_2/ZnO heteronanostructures are broadened greatly, suggesting that both SnO_2 and ZnO in 2D net-like heteronanostructures have smaller crystal sizes than those in 2D net-like homonanostructures, respectively. According to the Scherrer equation (D=0.9λ/Bcosϑ, where D is the crystallite size, B is full width at half maximum, ϑ is diffraction angle and λ is the wavelength of X-ray) the crystallite sizes of SnO_2 and ZnO in the net-like homonanostructures are estimated to be 7.3 and 23.8 nm, respectively (Tables S1).† However, the crystal sizes of SnO_2 and ZnO in the net-like heterostructures decrease to 2.3 and 9.3 nm, respectively (Tables S1).† The decreased sizes of both SnO_2 and ZnO facilitate the improvement of the sensing properties of the net-like heteronanostructures.

Another advantage of the present method is that the three as-synthesized samples can possess similar morphologies to grapehene sheets, as shown in low-magnification SEM images (Figure 2a), c) and e)).[39] The high-magnification SEM images (Figure 2b), d) and f)) show that these net-like nanostructures are composed of interconnected small nanoparticles, forming 2D porous structures. The porous features can make the nanoparticles contact with the target gases fully, and allow more target gas molecules to diffusion in or out the sensing films, which boost the sensitivity and shorten response and recovery times of the sensors.[10-14, 28, 30] Furthermore, from the SEM images it can be obviously found that the sizes of the nanoparticles in the net-like heteronanostructures are greatly smaller than those in the net-like homonanostructures, which is consistent with the XRD results.

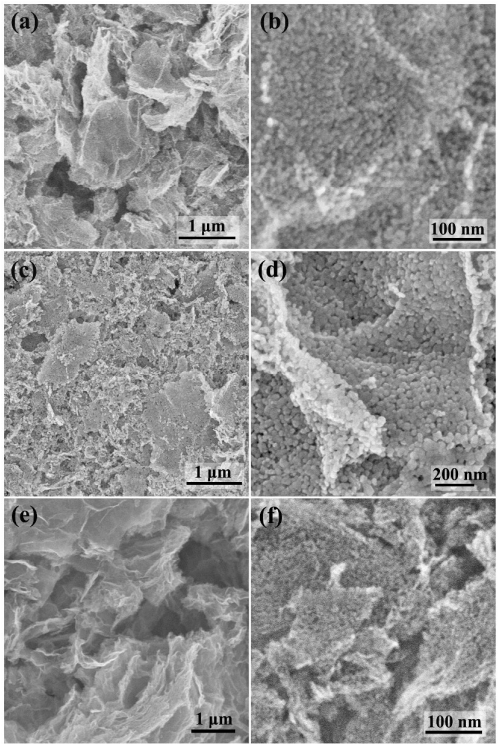

Figure 2 Low-magnification and high-magnification of SEM images of the 2D net-like nanostructures. (a,b) SnO_2 homonanostructures, (c, d) ZnO homonanostructures, and (e,f) SnO_2/ZnO heteronanostructures.

The structural features of the net-like samples were further confirmed by TEM observations. Figure 3a) displays a low-magnification TEM image of net-like SnO_2 homonanostructures, showing a net-like morphology of 2D SnO_2 homonanostructures with small pores in the plane. The size of the pores is in range of several nanometer to 50 nm, as shown in a magnification TEM image (Figure 3b)). Based on the measurements on more than 100 nanoparticles by means of TEM observation, we found that the percentages of SnO_2 nanoparticles with diameters in the ranges of 1–5, 5–10, 10–15, and >15 nm were about 16, 60, 22 and 2%, respectively. The marked diffraction rings in the selected-area electron diffraction (SAED) pattern (the inset in Figure 3(c)) correspond to the (110), (101) and (211) crystalline planes of tetragonal SnO_2, respectively. Diffraction dots or rings from other materials are not observed in the SAED pattern, further

demonstrating a high phase purity of SnO_2 in the net-like homonanostructures. Interestingly, the nanoparticles are interconnected tightly, suggesting that homojunctions will be formed at the interfaces between the neighboring particles. This is evidenced by high-resolution TEM (HRTEM) image (Figure 3c)), in which the lattice defects such as lattice distortion marked by red frames can be clearly observed in the region near the interfaces. The HRTEM image also reveals a highly crystallization degree of individual SnO_2 nanoparticles, in which the distances of the some adjacent lattice fringes, corresponding to different crystal planes of tetragonal SnO_2, are marked.

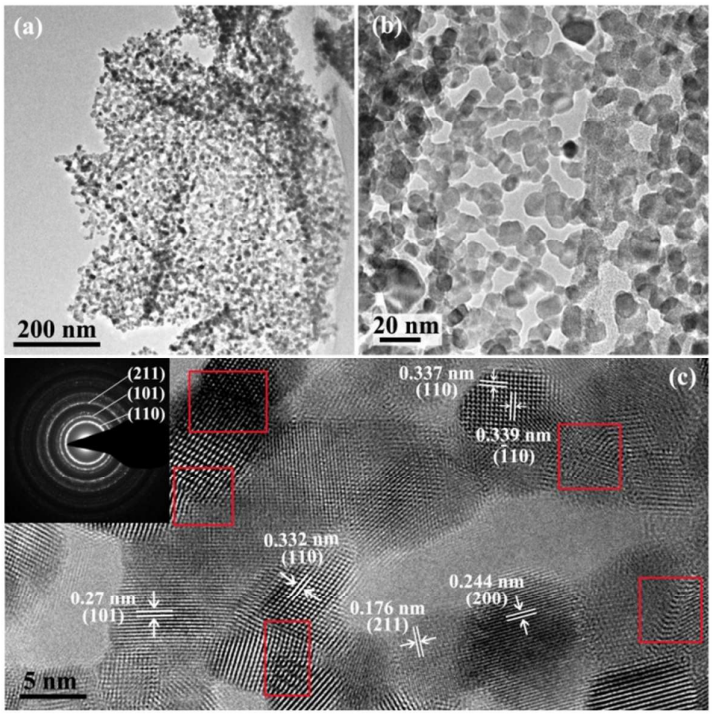

Figure 3 TEM images of the net-like SnO_2 homonanostructures. a) Low-magnification TEM image, b) high-magnification TEM image and c) HRTEM image, the inset in c) showing the corresponding SAED pattern, and the red frames showing the lattice defects in the homonanostructures.

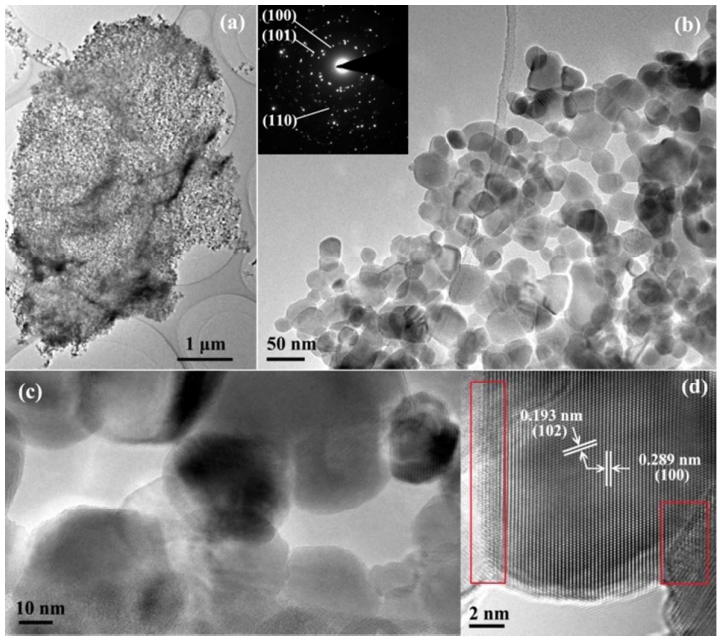

Figure 4 TEM images of the net-like ZnO homonanostructures. a) Low-magnification TEM image, b,c) high-magnification TEM image and d) HRTEM image, the inset in b) showing the corresponding SAED pattern, and the red frames showing the lattice defects at the interfaces.

Journal Name

ARTICLE

TEM images (Figure 4a) and b)) show that ZnO homostructures exhibit a net-like morphology with a porous feature, similar to those 2D SnO_2 homonanostructures possessed. However, the size of ZnO is greatly larger than that of SnO_2, as shown in Figure 4b) and 4c). Statistical result in terms of TEM observations shows that the percentages of ZnO nanoparticles with diameters in the ranges of 15–20, 20–30, 30–40, and 40–60 nm are about 30, 37, 21 and 12%, respectively. SAED pattern (the inset in Figure 4b)) and HRTEM image (Figure 4d)) demonstrate a crystal nature of individual ZnO nanoparticles. The lattice spacing values labeled in Figure 4d) are about 0.193 and 0.289 nm, corresponding to (102) and (100) crystal planes of hexagonal ZnO, respectively. Similarly, the lattice defects such as lattice distortion marked by red frames can be clearly observed near the interfaces, suggesting that homojunctions are also formed in the net-like ZnO homonanostructures.

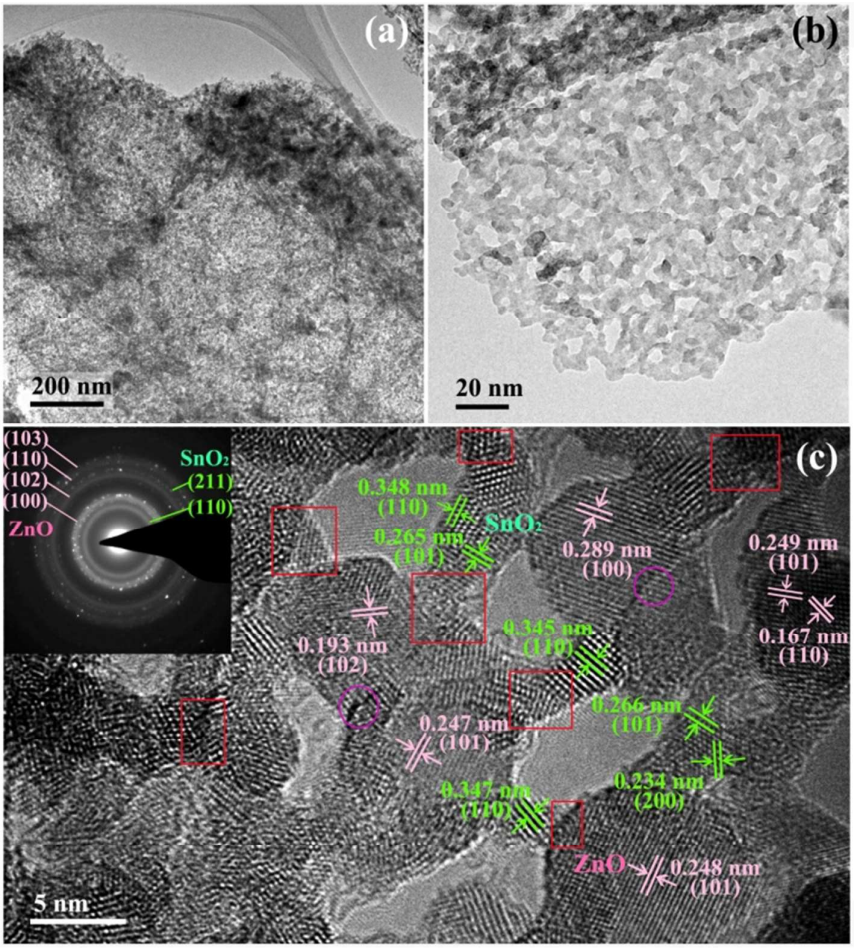

Figure 5 TEM images of the net-like SnO_2/ZnO heteronanostructures. a) Low-magnification TEM image, b,c) high-magnification TEM image and d) HRTEM image, the inset in b) showing the corresponding SAED pattern.

Similar to 2D SnO_2 and ZnO homonanostructures, SnO_2/ZnO heteronanostructures also exhibit a net-like morphology with a porous feature, as shown in Figure 5 a) and b). Diffraction rings from both SnO_2 and ZnO are presented in the SAED pattern (the inset in Figure 5c)), further confirming that the heteronanostructures are composed of SnO_2 and ZnO. The atomic ratio of Sn to Zn was determined by statistical energy dispersive X-ray spectrometry (EDX) results (Figure S1) to be about 0.9:1, close to the value (0.85:1) determined by inductively coupled plasma (ICP) mass spectrometry.† HRTEM

Journal Name

ARTICLE

image (Figure 5c)) shows that there are two kinds of nanoparticles with different sizes in the net-like heteronanostructures. The large nanoparticles exhibit a spherical shape, whereas the small nanoparticles show a strip-like morphology. XRD result reveals that the size of SnO2 is great larger than that of ZnO in the heteronanostructures, and thus we can safely conclude that the large and small nanoparticles are ZnO and SnO_2, respectively. This is further confirmed by HRTEM observations (Figure 5c)). As shown in the HRTEM image, the labeled *d*-spacings between the adjacent lattice fringes for large and small nanoparticles can be indexed to the crystal planes of hexagonal ZnO and tetragonal SnO_2, respectively. The lattice defects such as lattice distortion marked by red frames are observed among the adjacent ZnO and SnO_2 nanoparticles, suggesting that the heterointerfaces are formed in the net-like heteronanostructures. Besides, the homojuctions are also presented, as marked by the purple circles. Notably, Statistical result in terms of TEM observations shows that the average diameters of ZnO and SnO_2 are about 10.0 and 2.6 nm, respectively. Therefore, according to TEM and XRD results, the sizes of both SnO_2 and ZnO in the heteronanostructures are greatly decreased compared to those in the corresponding homonanostructures. This demonstrates that the introduction of ZnO can limit efficiently the growth of both SnO_2 and ZnO nanoparticles in the net-like heteronanostructures.

The SEM and TEM observations show that the net-like structures with a porous character consists of small nanoparticles, suggesting they have large surface areas. In terms of its nitrogen adsorption–desorption isotherms (Figure S2), Brunauer–Emmett–Teller (BET) surface areas of SnO_2 homonanostructures, ZnO homonanostructures, and SnO_2/ZnO heteronanostructures were calculated to be 54.6, 21.3, and 128.1 $m^2\ g^{-1}$, respectively.† The average pore diameter and cumulative volume of pores calculated from the adsorption branch of the nitrogen isotherm using the Barrett–Joyner–Halenda (BJH) method (the insets in Figure S2) are about 20.2 nm and 0.27 $cm^3\ g^{-1}$ for SnO_2 homonanostructures, 21.2 nm and 0.07 $cm^3\ g^{-1}$ for ZnO homonanostructures, and 11.1 nm and 0.42 $cm^3\ g^{-1}$ for SnO_2/ZnO heteronanostructures, respectively.

We used graphene sheets as hard templates to synthesize 2D net-like SnO_2/ZnO heteronanostructures with a porous feature in the present work. In terms of the experimental results above, we found that the size of SnO_2 was suppressed significantly by the introduction of foreign ZnO materials. Thus the amount of ZnO in the G/SnO_2/ZnO precursor may have an important role in the final morphology of the heteronanostructure. As demonstrated in the experimental section, the above 2D net-like SnO_2/ZnO heteronanostructures with an atomic ratio of Sn to Zn of about 0.9:1, denoted as SZ-1 for convenience, could be obtained as the addition amount of zinc acetate was 0.7 g. The sample with an increased atomic ratio of Sn to Zn, denoted as SZ-2, could be obtained if decreased to 0.175 g. The atomic ratio of Sn to Zn is determined to about 1.2:1 by EDS ananlyses (Figure S3a).† SZ-2 also exhibits 2D net-like morphology (Figure S3b)); however, compared to SZ-1, the pore size in SZ-2 is slightly increased (Figure S3c).† Furthermore, the heterointerfaces are also formed, as shown in Figure S3d).† On the other hand, in order to decrease the atomic ration of Sn to Zn in the heteronanostructures G/SnO_2/ZnO composite was stirred in the zinc acetate solution again for 10 h. After heating the composite at 500°C for 3 h, the obtained sample is denoted as SZ-3. EDS analysis shows that the atomic ration of Sn to Zn in SZ-3 is around 0.7:1 (Figure S4a).† Similar to S1 and S2, SZ-3 also shows 2D net-like structures (Figure S4b); however, the pore size is samller than that in S1 and S2 due to higher density of the nanoparticles (Figure S4c and d)).† In addition, the heterointeraces are also formed in the 2D nanostructures, as shown in Figure S4d).† Noted that the SnO_2 and ZnO in these heteronanostructures have little change in size, revealing that the amount of the foreign ZnO mainly has effect on the pore size in the heteronanostruces as well as the number of heterointeraces.

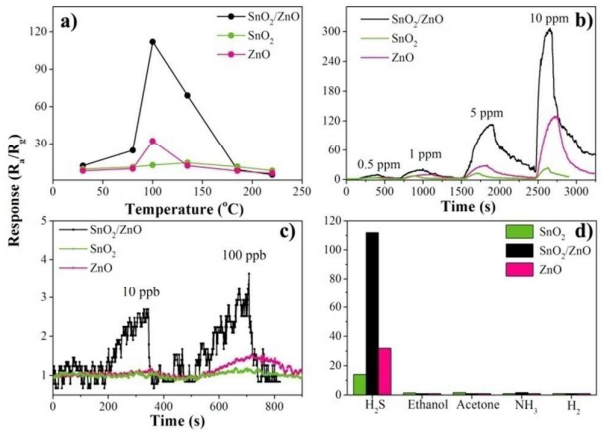

Figure 6 H_2S sensing properties of the net-like SnO_2 and ZnO homonanostructuresm and SnO_2/ZnO heteronanostructures. a) Sensor responses of the nanostructures to 5 ppm H_2S gases at various working temperatures, b) Time-dependent sensor responses of the nanostructures at 100°C, c) Time-dependent sensor responses of the nanostructures to 10 and 100 ppb H_2S at 100°C, and d) selectivity of the nanostructures, the working temperature is 100 °C, the concentration of H_2S is 5 ppm, and the concentrations of other types of gases are 100 ppm.

Because the net-like SnO_2/ZnO heteronanostructures have bigger surface area and heterointerfaces, they may show better gas sensing performance than those of SnO_2 and ZnO homonanostructures. Figure 6a) shows sensor responses of the three net-like nanostructures to 5 ppm H_2S gas at various working temperatures. It can be found that the net-like SnO_2/ZnO heteronanostructures have larger sensor response values than those of SnO_2 and ZnO homonanostructures at all the tested temperatures. For example, the sensor response for net-like SnO_2/ZnO heteronanostructures to 5 ppm H_2S at 100°C is about 112, whereas the values are only about 32 and 12 for SnO_2 and ZnO homonanostructures, respectively. From the Figure, it can be found that the optimum operating temperature of the sensors is 100°C. In general, sensing materials based on MOSs showed a maximum sensor response to the reducing gas with a given concentration at an optimum working temperature. [40-42] At room temperature the sensor response is relatively low. As the working temperature increases, sensor response will increase due to the activation of adsorbed molecular oxygen and lattice oxygen to form oxygen ions. This phenomenon will last until an optimum working temperature is achieved, after that exothermic gas adsorption is difficult and the gas molecule desorption becomes a predominant behavior, leading to a decreased sensor response. In addition, the optimum working temperature is also dependent on the size, structure, phase and morphology of sensing materiales.[40-42] Considering the following factors, it is reasonable that the heteronanostructures can detect H_2S gas at 100°C. First, both SnO_2 and ZnO nanostructures have responses to H_2S gas at the working temperature ranging from room temperature to 300°C.[32-34,41] Second, the both SnO_2 and ZnO in the heteronanostructures have small sizes. It is well known that the small size effect facilitates the decrease of the working temperature due to high surface energy of MOS with a small size.[42] Third, the metal oxides in the heteronanostructures may react with H_2S at 100°C, and then transform to metal sulfides. Such transformation can improve the sensitivity and selectivity of the heteronanostructures to H_2S gas, which will further discuss later.

To further investigate the H_2S sensing performance of the net-like nanostructures, we also measured their time-dependent responses to H_2S gases with different concentrations at the optimum operating temperature. As shown in Figure 6b), the response values of the net-like SnO_2/ZnO heteronanostructures to all the tested H_2S concentrations (0.5–10 ppm) are significantly larger than those of SnO_2 and ZnO homonanostructures at the optimum operating temperature. Therefore, the net-like SnO_2/ZnO heteronanostructures exhibit enhanced H_2S sensing properties. Furthermore, both SnO_2 and ZnO homonanostructures have a weak response to 100 ppb H_2S; however, the net-like SnO_2/ZnO heteronanostructures have a distinct response even to 10 ppb H_2S, as shown in Figure 6c). Compared to other H_2S sensing materials, the net-like SnO_2/ZnO heteronanostructures exhibit better H_2S sensing properties including larger response value, lower detection limit and lower working temperature, summarized in Table S2.† Noted that the heteronanostructures exhibited a relatively long recovery time to H_2S gas with a high concentration at a low working temperature of 100°C, which may be due to numerous adsorption of H_2S molecules and a relatively low surface reaction kinetics at a low working temperature.[32-34] For example, the recovery time of the heteronanostructure to 5 ppm H_2S is about 513 s. The recovery time could be decreased by increasing the working temperature. As shown in Figure S5, the recovery time can be decreased to 98 s, but the increased temperature will lead to a significant decrease in the sensor response.† Nevertheless, the heteronanostructures showed a short response time to H_2S gas with a low concentration at 100°C. For example, the recovery times of the heteronanostructures to both 10 and 100 ppb H_2S are less than 40 s (Figure 6c)). The results above demonstrates that the net-like SnO_2/ZnO heteronanostructures are very promising sensing materials for high-performance H_2S sensors.

The gas sensors for practical applications are required not only to have strong response, but also to have a very good selectivity to the targeted gas. Therefore, we examined the responses of the net-like nanostructures to 100 ppm acetone, 100 ppm H_2, 100 ppm ethanol and 100 ppm NH_3 at 100°C. As shown in Figure 6d), the sensor response of the net-like heteronanostructures to 5 ppm is about 112, however, the response values are negligible even to 100 ppm other four gases. Thus, the net-like SnO_2/ZnO heteronanostructures have good selectivity to H_2S gas. The reasons for the good selectivity are relatively complicated. First, when the net-like nanostructures are exposed to the reducing gases such as H_2S, ethanol, H_2 and NH_3, the gases will react with chemisorbed oxygen species on the surfaces of the sensing materials. The corresponding surface reaction kinetics is quiet different, leading to different sensor response of the heteronanostructures to different gases.[9-29] Second, the metal oxides may react with H_2S, resulting in the formation of a little amount of metal sulfides in the surface.[40,43] The conductivity of metal sulfide is higher than that of the corresponding metal oxide.[44-46] This leads to larger variation in the surface resistance. Thus the heteronanostructures exhibited good selectivity to H_2S. To provide the evidence for the assumption, XPS spectra were collected from the heteronanostructures before and after H_2S sensing test (exposure to 10 ppm H_2S at a working temperature of 100°C for 10 min.). As shown in Figure S6a), the peaks related to S species are not found in the XPS spectrum of the heteronanostructures before H_2S sensing test, however, after H_2S sensing measurement a weak peak located at 162.1 eV corresponding to $S^{(II)}$ species appears.[44-46] Furthermore, EDS patterns (Figure S7) also demonstrate that small amount of S species is presented in the heteronanostructure after H_2S sensing test.† Thus, the transformation of metal oxide to metal sulfide is attributed to the good selectivity of the heteronanostructures to H_2S. This also implies that, besides physical adsorption, chemical adsorption is also involved in the H_2S sensing process. However, the detailed adsorption steps need to be further

studied. In addition, the peak positions of Sn and Zn species and the atomic ratio of Sn to Zn have little changes, implying the structural stability of the heteronanostructures as H_2S sensing materials (Figure S6b) and c)).† Noted that the transformation of metal oxide to metal sulfide is reversible, i.e., metal sulfide can also convert to metal oxide as the sensing heteronanostructures exposed to air atmosphere at the working temperature (100°C). The peak relative to S species disappears in the EDS pattern of the heteronanostructures after 1 ppm H_2S testing, and then exposing air at 100°C until the sensor resistance recovers to more than 90% of the initial resistance (Figure S8). This supports the reversible transformation. However, the sluggish kinetics of the transformation reaction leads to a long recovery time of the H_2S sensor (Figure 6b)).†

In addition, the long-term stability of the net-like heteronanostructures was also measured. As shown in Figure S9, the sensor responses to 5 ppm H_2S at 100°C are kept the response values with little fluctuation for 60 days of testing, suggesting they have a good stability.† The high sensor response, good selectivity and long-term stability of the net-like heteronanostructures demonstrate that they have very promising applications in H_2S gas sensors. After the long-term H_2S measurements, the structures of the heteronanostructures were characterized by SEM and TEM measurements. Although the sizes of the nanoparticles in the heteronanostructures are increased slightly (Figure S10a) and c)), their 2D net-like morphologies were well kept (Figure S10b and c)), revealing the structural stability of the heteronanostructures as H_2S sensing materials.†

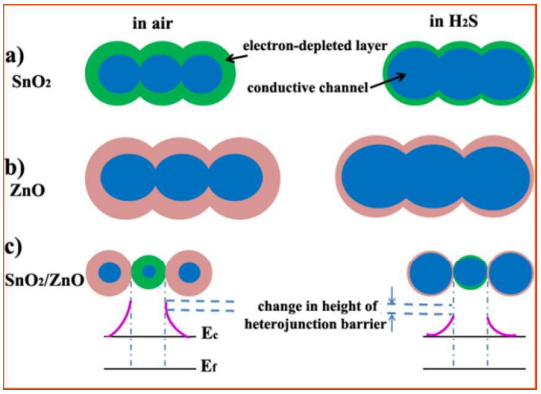

Figure 7 Illustration of the enhanced sensing mechanism of the 2D net-like heteronanostructures. a) and b) The sensing mechanisms about pure SnO_2 and ZnO with larger size, respectively, and c) the sensing mechanism about the net-like SnO_2/ZnO heteronanostructures.

The enhanced sensing mechanism of the net-like SnO_2/ZnO heteronanostructures can be attributed to the following facts. Firstly, both SnO_2 and ZnO in the net-like SnO_2/ZnO heteronanostructures have smaller sizes than those in the homonanostructures. The small size effect will improve the sensing property of the net-like SnO_2/ZnO heteronanostructures greatly. For MOS, the size is smaller than the Debye length (λ_D), the MOS will be completely electron-depleted in air by the adsorption of oxygen species and is highly resistive. As MOS is exposed to the reducing gases, the reducing gases will react with the adsorbed oxygen species, and then the depleted electrons will be released back to MOS. Consequently, in this case the resistance of MOS has a very large variation. However, if the size is larger than the Debye length, the resistance of MOS at air and reducing gases will show a smaller change.[4,22,47] Thus, MOS with a small size close to its Debye length is highly desirable to improve its sensitivity to reducing gases. λ_D for an oxide material can be calculated by the following equation:[48]

$$\lambda_D = (\varepsilon kT/q^2 n_c)^{1/2} \quad (1)$$

where ε, k, T, q, and n_c are the static dielectric constant, Boltzmann's constant, the absolute temperature, the electrical charge, and the carrier charge concentration, respectively. According to the equation, λ_D for SnO_2 is estimated to be around 3 nm, whereas it is around 20 nm for ZnO.[4,22,48] In terms of XRD and TEM analyses, the sizes of most SnO_2 nanoparticles in the net-like SnO_2 homonanostructures are larger than 3 nm, whereas those in the SnO_2/ZnO heteronanostructures have sizes close to 3 nm. Similarly, most ZnO nanoparticles in the net-like ZnO homonanostructures have sizes larger than the Debye length of ZnO, whereas those in the SnO_2/ZnO heteronanostructures have size smaller than the Debye length of ZnO. Thus the enhanced sensing properties of the SnO_2/ZnO heteronanostructures can be attributed to the small size effect, as shown in Figure 7a), b) and c). Secondly, due to different electron work function of ZnO (5.2 eV) than that of SnO_2 (4.9 eV), as the tight interfaces are efficiently formed among the adjacent ZnO and SnO_2 nanoparticles, the unidirectional flow of electrons will occur until the built-up electric field prevents it. This results in the generation of heterojunction barriers at the interfaces between the two materials.[22, 47] In air, the height of the heterojunction barriers is increased because electrons are trapped both in SnO_2 and ZnO induced by adsorbed oxygen species, as shown in Figure 7c). In this case, the conductivity of the heteronanostructures is very low. When the heterostructures are exposed to H_2S, the reaction between the adsorbed oxygen species and the H_2S molecules leads to the release of the trapped electrons back simultaneously into the conduction bands of the SnO_2 and ZnO, decreasing the height of the barrier potential at the interfaces, as shown in Figure 7c). Consequently, the conductivity of the heteronanostructures will be greatly increased; resulting in the enhanced sensitivity of the heteronanostructures to H_2S.[25] Therefore, the change in the height and width of the heterojunction barriers at different gas atmospheres contributes to the enhanced sensing properties of the SnO_2/ZnO heteronanostructures.

4 Conclusions

In summary, the SnO_2/ZnO heteronanostructures with a porous feature were successfully fabricated by a facile method. As applied as H_2S gas sensors, they exhibited high sensor response, good selectivity and long-term stability. Importantly, the SnO_2/ZnO heteronanostructures can detect

10 ppb H_2S gas at a relatively low working temperature (100˚C). Furthermore, compared to SnO_2 and ZnO homonanostructures, and other types of MOSs, SnO_2/ZnO exhibited enhanced H_2S sensing properties, which can be attributed to the small size effect and the formation of heterojunctions at the interfaces. Our results indicate that the net-like SnO_2/ZnO heteronanostructures are good candidates for high-performance H_2S sensors. Furthermore, the fabrication method may be extended to synthesize other 2D net-like metal oxides for applications in various fields.

Acknowledgements

We thank the National Natural Science Foundation of China (Grant no. 51272050 and 51572051), the Innovation Foundation of Harbin City (2012RFXXG096), the 111 project (B13015) of the Ministry of Education of China to the Harbin Engineering University, and also supported by the Open Project Program of Key Laboratory for Photonic and Electric Bandgap Materials, Ministry of Education, Harbin Normal University, China.

Notes and references

1 N. L. Wu, S. Y. Wang and I. A. Rusakova, Science, 1999, **285**, 1375.
2 M. Law, H. Kind, G. Messer, F. Kim and P. D. Yang, Angew. Chem. Int. Ed., 2002, **41**, 2405.
3 C. Nayral, T. Ould-Ely, A. Maisonnat, B. Chaudret, P. Fau, L. Lescouzeres and A. Peyre-Lavigne, Adv. Mater., 1999, **11**, 61.
4 Y. J. Chen, L. Nie, X. Y. Xue, Y. G. Wang and T. H. Wang, Appl. Phys. Lett., 2006, **88**, 083105.
5 C. N. Xu, J. Tamaki, N. Miura and N. Yamazoe, Sens. Actuators, B, 1991, **3**, 147.
6 E. Comini, G. Faglia, G. Sberveglieri, Z. W. Pan and Z. L. Wang, Appl. Phys. Lett., 2002, **81**, 1069.
7 H. Ogawa, M. Nishikawa and A. J. Abe, Appl. Phys.,1982, **53**, 4448.
8 N. Barsan and U. J. Weimar, Electroceram, 2001, **7**, 143.
9 Y. J. Chen, G. Xiao, T. S. Wang, F. Zhang, Y. Ma, P. Gao, C. L. Zhu, E. Zhang, Z. Xu and Q. H. Li, Sens. Actuators, B, 2011, **155**, 270.
10 C. L. Zhu, H. L. Yu, Y. Zhang, T. S. Wang, Q. Y. Ouyang, L. H. Qi, Y. J. Chen and X. Y. Xue, ACS Appl. Mater. Interfaces, 2012, **4**, 665.
11 P. Sun, X. Zhou, C. Wang, K. Shimanoe, G. Lu and N. Yamazoe, J. Mater. Chem. A, 2014, **2**, 1302.
12 X. Zhou, W. Feng, C. Wang, X. L. Hu, X. W. Li, P. Sun, K. Shimanoe, N. Yamazoe and G. Lu, J. Mater. Chem. A, 2014, **2**, 17683.
13 X. M. Gao, C. Y. Li, Z. X. Yin and Y. J. Chen, RSC Adv., 2015, **5**, 37703.
14 A. Katoch, J. H. Kim and S. S. Kim, ACS Appl. Mater. Interfaces, 2014, **6**, 21494.
15 Y. V. Kaneti, M. Quadir, D. Zakaria, Z. J. Zhang, C. Y. Chen, J. Yue, M. S. Liu, X. C. Jiang and A. B. Yu, J. Mater. Chem. A, 2014, **2**, 13283.
16 W. Q. Li, S. Y. Ma, Y. F. Li, G. J. Yang, Y. Z. Mao, J. Luo, D. J. Gengzang, X. L. Xu and S. H. Yan, Sens. Actuators, B, 2015, **211**, 392.
17 H. Huang, H. Gong, C. L. Chow, J. Guo, T. J. White, M. S. Tse and O. K. Tan, Adv. Funct. Mater., 2011, **21**, 2680.
18 J. L. Zhai, L. L. Wang, D. J. Wang, H. Y. Li, Y. Zhang, D. Q. He and T. F. Xie, ACS Appl. Mater. Interfaces, 2011, **3**, 2253.
19 Y. J. Chen, F. N. Meng, C. Ma, Z. W. Yang, C. L. Zhu, Q. Y. Ouyang, P. Gao, J. Q. Li and C. W. Sun, J. Mater. Chem., 2012, **22**, 12900.
20 L. Yin, D. L. Chen, M. X. Hu, H. Y. Shi, D. W. Yang, B. B. Fan, G. Shao, R. Zhang and G. S. Shao, J. Mater. Chem. A, 2014, **2**, 18867.
21 T. S. Wang, Q. S. Wang, C. L. Zhu, Q. Y. Ouyang, L. H. Qi, C. Y. Li, G. Xiao, P. Gao and Y. J. Chen, Sens. Actuators, B, 2012, **171**, 256.
22 A. Katoch, J. Kim, Y. Kwon, H. Kim and S. Kim, ACS Appl. Mater. Interfaces, 2015, **7**, 11351.
23 A. Katoch, S. Choi, J. Kim, J. H. Lee, J. Lee and S. S. Kim, Sens. Actuators, B, 2015, **214**, 111.
24 C. Wang, J. Zhu, S. Liang, H. Bi, Q. Han, X. Liu and X. Wang, J. Mater. Chem. A, 2014, **2**, 18635.
25 L. Wang, J. Deng, Z. Lou and T. Zhang, J. Mater. Chem. A, 2014, **2**, 10022.
26 D. Bekermann, A. Gasparotto, D. Barreca, C. Maccato, E. Comini, C. Sada, G. Sberveglieri, A. Devi and R. A. Fischer, ACS Appl. Mater. Interfaces, 2012, **4**, 928.
27 L. Zhang, Z. Gao, C. Liu, Y. Zhang, Z. Tu, X. Yang, F. Yang, Z. Wen, L. Zhu, R. Liu, Y. Li and L. Cui, J. Mater. Chem. A, 2015, **3**, 2794.
28 K. Choi, H. Kim, Y. C. Kang and J. Lee, Sens. Actuators B, 2014, **194**, 371.
29 J. Deng, L. Wang, Z. Lou and T. Zhang, J. Mater. Chem. A, 2014, **2**, 9030.
30 Y. J. Chen, X. M. Gao, X. P. Di, Q. Y. Ouyang, P. Gao, L. H. Qi, C. Y. Li and C. L. Zhu, ACS Appl. Mater. Interfaces, 2013, **5**, 3267.
31 M. S. Wagh, L. A. Patil, T. Seth and D. P.Amalnerkar, Mater. Chem. Phys., 2004, **84**, 228.
32 Y. L. Cao, D. Z. Jia, R. Y. Wang and J. M. Luo, Solid-State Electron., 2013, **82**, 67.
33 H. Kim, C. Jin, S. Park and C. Lee, Mater. Res. Bull., 2012, **47**, 2708.
34 P. S. Shewale, Y. S. Yu, J. H. Kim, C. R. Bobade and M. D. Uplane, J. Anal. Appl. Pyrol., 2015, **112**, 348.
35 Y. J. Chen, C. L. Zhu, L. J. Wang, P. Gao, M. S. Cao and X. L. Shi, Nanotechnology, 2009, **20**, 045502.
36 Y. L. Ren, H. Y. Wu, M. M. Lu, Y. J. Chen, C. L. Zhu, P. Gao, M. S. Cao, C. Y. Li and Q. Y. Ouyang, ACS Appl. Mater. Interfaces, 2012, **4**, 6436.
37 Q. Y. Ouyang, Z. Xu, Z. Y. Lei, H. W. Dong, H. L. Yu, L. H. Qi, C. Y. Li and Y. J. Chen, Carbon, 2014, **67**,214.
38 Y. J. Chen, G. Xiao, T. S. Wang, F. Zhang, Y. Ma, P. Gao, C. L. Zhu, E. D. Zhang, Z. Xu and Q. H. Li, Sens. Actuators, B, 2011, **156**, 867.
39 H. Zhang, C. Zhu, Y. Chen, M. Yang, P. Yang, X. Wu, L. Qi and F. Meng, J. Mater. Chem. A, 2015, 3, 1421.
40 Y. F. Sun, S. B. Liu, F. L. Meng, J. Y. Liu, Z. Jin, L. T. Kong and J. H. Liu, Sensors, 2012, **12**, 2610-2631.
41 K. Diao, M. Zhou, J. Zhang, Y. Tang, S. Wang and X. Cui, Sens. Actuators B, 2015, **219**, 30-37.
42 K. Wetchakun, T. Samerjai, N. Tamaekong, C. Liewhiran, C. Siriwong, V. Kruefu, A. Wisitsoraat, A. Tuantranont, S. Phanichphant, Sens. Actuators B, 2011, **160**, 580.
43 J. H. Lee, Sens. Actuators B, 2009, **140**, 319-336.
44 G. Qi, L. Zhang and Z. Yuan, *Phys. Chem. Chem. Phys.*, 2014, **16,** 13434-13439.
45 W. Luo, J. Deng, Q. Fu, D. Zhou, Y. Hu, S. Gong and Z. Zheng, Sens. Actuators B, 2015, **217**, 119-128.
46 H. Huang, P. Xu, D. Zheng, C. Chen and X. Li, J. Mater. Chem. A, 2015, **3**, 6330-6339.
47 S. –W. Choi, A. Katoch, C. –J. Sun, J. –H. Kim, S. –H. Kim and S. S. Kim, ACS Appl. Mater. Interfaces, 2014, **6**, 8281.
48 S. M. Sze, Physics of Semiconductor devices, 2nd et., Wiley-Interscience: Singapore, 1936; Chapter **2**, 63-132.

49 R. Zou, G. He, K. Xu, Q. Liu, Z. Zhang and J. Hu, J. Mater. Chem. A, 2013, **1**, 8445.
50 Z. Zhang, R. Zou, G. Song, L. Yu, Z. Chen and J. Hu, J. Mater. Chem., 2011, **21**, 17360.
51 L. Yin, D. Chen, X. Cui, L. F. Ge, J. Yang, L. Yu, B. Zhang, R.Zhang and G. Shao, *Nanoscale*, 2014, **6**, 13690.
52 S. Bai, C. Chen, R. Luo, A. Chen and D. Li, *Sens. Actuators, B*, 2015, **216**, 113.
53 X. Zhou, Y. Xiao, M. Wang, P. Sun, F. Liu, X. Liang, X. Li and G. Lu, *ACS Appl. Mater. Interfaces*, 2015, **7**, 8743.
54 J. Ma, Y. Liu, H. Zhang, P. Ai, N. Gong, Y. Wu and D. Yu, *Sens. Actuators, B*, 2015, **216**, 72.
55 S. Zhang, P. Zhang, Y. Wang, Y. Ma, J. Zhong and X. Sun, *ACS Appl. Mater. Interfaces*, 2014, **6**, 14875.
56 F. E. Annanouch, Z. Haddi, S. Vallejos, P. Umek, P. Guttmann, C. Bittencourt and E. Llobet, *ACS Appl. Mater. Interfaces*, 2015, **7**, 6842.
57

Net-like SnO_2/ZnO heteronanostructures with a porous feature and heterojunctions at the interfaces were successfully designed and fabricated by a facile method. Importantly, they could detect 10 ppb H_2S even at a working temperature of 100°C.